JGR Planets

RESEARCH ARTICLE
10.1029/2022JE007316

Key Points:

- Layer formation is possible in a subsurface ocean that is heated from below, enriched in salts at the bottom and fresher on top
- Layering is a transient feature, but this can be long lasting if the concentration difference between the top and bottom is large
- As heat and material transport is inhibited while layers exist, the subsurface ocean may not be efficient in transport

Supporting Information:

Supporting Information may be found in the online version of this article.

Correspondence to:

T. Wong,
t.wong@uni-muenster.de

Citation:

Wong, T., Hansen, U., Wiesehöfer, T., & McKinnon, W. B. (2022). Layering by double-diffusive convection in the subsurface oceans of Europa and Enceladus. *Journal of Geophysical Research: Planets*, *127*, e2022JE007316. https://doi.org/10.1029/2022JE007316

Received 13 APR 2022
Accepted 17 NOV 2022

Layering by Double-Diffusive Convection in the Subsurface Oceans of Europa and Enceladus

Teresa Wong[1], Ulrich Hansen[1], Thomas Wiesehöfer[1], and William B. McKinnon[2]

[1]Institut für Geophysik, Westfälische Wilhelm-Universität Münster, Münster, Germany, [2]Department of Earth and Planetary Sciences, Washington University in St. Louis, St. Louis, MO, USA

Abstract Subsurface oceans rich in salts may be prevalent in the icy worlds of the outer solar system. Surface observations have led to various hypotheses for the transport of materials from the seafloor to the surface by hydrothermal plumes, and raise questions about heat transfer mechanisms. Chemical heterogeneity affects the vigor of convection, the forms of plumes, the generation and destruction of stratified or finger structures in the ocean, and thus the transport of heat and materials from the interior to the surface. Here, we investigate the layering phenomenon in a double-diffusive convection system, which can occur when both the temperature and concentration influence the density of the fluid. The persistence of layers may depend on the buoyancy ratio, the Rayleigh number, boundary conditions, and initial conditions, which alter the chemical distribution and thus the balance between thermal and chemical buoyancies. Our simulations suggest that the layering could exist for a longer duration if the buoyancy ratio is raised with boundary conditions that maintain a large concentration difference. When the layers are present, heat and material transport are significantly inhibited through the subsurface ocean from the silicate interior to the base of the icy shell.

Plain Language Summary The subsurface oceans of icy satellites are almost certainly salt to some degree, and this gives rise to the possibility of layering by the process of double-diffusive convection. The evolution of layers has long been a topic of interest for the terrestrial ocean, and under subsurface ocean conditions there are additional motives to study this phenomenon, as the layers can hinder heat and material transport and thus have to be taken into account when considering the evolution of the icy moons and what could be observed on the surface. We investigate the evolution of layers in a double-diffusive convection system, where both the temperature and the concentration affect the density of the fluid. We examine the development of the first and subsequent layers, how they emerge and finally disappear, and what could prolong their lifetimes.

1. Introduction

The prospect of subsurface oceans in icy satellites presents an exciting area of research to understand their diverse processes and astrobiological potential. Induced magnetic fields were detected by *Galileo* on Europa, Ganymede, and Callisto (Khurana et al., 2009; Kivelson et al., 2000; Zimmer et al., 2000), which implies a subsurface ocean. Gravity measurements and surface features indicate that the icy shells are decoupled from the interior (cf. Hussmann et al., 2015). Direct imaging of erupting plumes on Enceladus from Cassini and potentially on Europa as well, from Hubble Space Telescope and magnetic field and plasma wave observations from *Galileo* (Jia et al., 2018) point to subsurface water sources. The surface observations offer clues about the composition of the subsurface ocean. Measurements of Saturn's E-ring indicate a sodium salt-rich source derive from Enceladus' interior (e.g., Postberg et al., 2009). Spectroscopic data from *Galileo*'s NIMS suggests the presence of irradiated salts on the surface of Europa that may reflect the composition of the subsurface ocean (McCord et al., 1998; Trumbo et al., 2019). This non-water ice material is prominent in linear and chaos features on the surface. What are the sources of these salty materials? Can their presence on the surface reflect the composition in greater depths, for example, from the subsurface ocean or even from the silicate interior? How are they transported to the surface, and is the dynamics in the subsurface ocean expressed on the surface?

Current understanding of icy subsurface oceans is drawn from studies of the Earth's ocean, fundamental knowledge of geophysical fluid dynamics, numerical simulations, and laboratory experiments. Topics of heat and material transport by hydrothermal systems and the circulation in the subsurface ocean have been explored with various assumptions about its conditions and physical properties (e.g., Amit et al., 2020; Goodman et al., 2004; Kvorka

& Čadek, 2022; Lowell & DuBose, 2005; Melosh et al., 2004; Soderlund, 2019; Thomson & Delaney, 2001; Travis et al., 2012; Vance & Brown, 2005; Zhu et al., 2017). The presence of salts may alter the behavior of ocean currents and plumes and prevent the ocean from being well-mixed, disturbing the transport of heat across the ocean. Much of the geochemistry is uncertain due to the lack of constraints on the conditions in the ocean (e.g., Zolotov & Kargel, 2009). Convection would play a role in setting the temperatures and oxidation states, affecting the water-rock interactions and thus the concentration distribution in the ocean. Global circulation models with parameterized mixing mechanisms have been used to simulate the subsurface ocean flows, exploring the effects of salinity on ocean dynamics and the interaction of the subsurface ocean with the surrounding layers (Ashkenazy & Tziperman, 2021; Bire et al., 2022; Kang et al., 2022; Zeng & Jansen, 2021).

Here, we study the mechanism of double-diffusive convection to understand the dynamics of the salty subsurface oceans, calculating explicitly the processes of advection, thermal and chemical diffusion. It is a well-developed concept in the context of oceanography (e.g., Radko, 2013, and references therein). Further geological applications include magma dynamics, global scale convection in planetary mantle and cores (e.g., Hansen & Yuen, 1995). It has been suggested that double-diffusive convection can occur in the subsurface oceans, and it may result in a layered structure, saline instabilities in finger shape or precipitation such as salt rain or salt snow (e.g., Vance & Brown, 2005; Vance & Goodman, 2009). Previous studies assessed the occurrence of double-diffusive convection as a possible mechanism affecting heat and material transport by analyzing the stability of the subsurface oceans mainly based on linear stability. However, the onset of convection predicted by linear theory has been shown to be inadequate for the nonlinear behavior of the fluid from laboratory and numerical experiments (Fernando, 1989a; Huppert & Moore, 1976).

Are there any conditions, for example, with changing temperatures and composition at the boundaries, in which layers can exist for a long time? Can the layers be sustained for a substantial part of the moon's history? What controls the formation of layers, and the duration of their existence? We perform numerical modeling of the evolution of the subsurface ocean with different boundary conditions to address these questions. This study focuses on subsurface oceans that are sandwiched in between an icy shell and a rocky interior, which are thought to be prevalent in many icy satellites. The considerations of boundary conditions are based on such a setting, which differentiates the subsurface oceans from the Earth's ocean. Here, we aim to demonstrate the phenomena and to lay the groundwork for further theoretical analysis of double-diffusive convection in a subsurface ocean setting.

2. Double-Diffusive Convection

Double-diffusive convection typically occurs if two components, such as heat and salt (composition), influence the density of the fluid in opposite ways. It is thus a mixing process driven by the interplay of thermal and chemical buoyancies. While heat acts to decrease the density (noting that the anomalous thermal expansion of water can, under certain circumstances, cause the opposite), the concentration of salt will increase the density of the fluid. The diffusivity of salt is many orders of magnitude smaller, which means the temperature of the perturbed fluid is adjusted much more rapidly to its surroundings than the concentration, such that the small diffusivity acts to preserve the concentration of the fluid. Compositional density differences may provide further driving or restoring forces in addition to those due to the thermal density difference in convection. If the driving force is dominant, the convection system is considered “supercritical”; otherwise, it is “subcritical.” Since the driving and stabilizing forces act on the fluid on different timescales, even if net-density stratification is stable under subcritical conditions, convection can still occur. Thus the concept of neutral buoyancy will have to take into account the nonlinear nature of double-diffusive convection.

Various phenomena can occur depending on the initial distribution of temperature and salts. In double-diffusive convection studies, these temperature and concentration distribution combinations are categorized into different regimes (see Hansen & Yuen, 1995). For example, salt fingers can develop in the regime where the warmer and more concentrated fluid is on top of the colder and dilute fluid under subcritical conditions, such that the slow diffusing component (e.g., salt) is the driving force while the fast diffusing component (temperature) acts as the greater restoring force. Such conditions exist in terrestrial oceans. On the other hand, when the colder and compositionally lighter (or less saline) fluid overlies a hotter and denser fluid, the temperature is the destabilizing force whereas the composition is the stabilizing force. This regime is termed the “diffusive” regime. In the diffusive regime under subcritical conditions, layers are known to form in a self-organized manner as they can evolve from

a concentration gradient without imposing a prior stratification of material or temperature. Layer formation in the diffusive regime is relevant at, for example, the polar latitudes of the Earth's ocean (e.g., Fernando, 1989a; Shibley et al., 2017; Spigel et al., 2018; Timmermans et al., 2017), and it is believed to happen in magmatic systems (Martin et al., 1987). In the scenario where a compositionally dense and cold fluid is on top of the light and hot fluid, convection is enhanced compositionally as both temperature and composition act as driving force. In the opposite case when a hot and light fluid is above the cold and dense fluid, both forces are restoring and convection ceases.

The subsurface oceans considered here differ from terrestrial oceans in their boundary conditions, as the ocean is buried under the ice and not in contact with an atmosphere. On the Earth, there are limited regions of the major oceans that satisfy the conditions for a diffusive regime (You, 2002). The thermal and chemical distribution in icy satellites may vary spatially and temporally. In this study, we construct simple systems to observe layering from double-diffusive convection, and to discuss the mechanisms of layer formation and breakdown and its consequences for the thermal evolution of the moons.

3. Numerical Model

We perform numerical calculations using a finite volume code for double-diffusive convection at finite Prandtl number, where the chemical constituent is treated in a field approach, meaning a further advection/diffusion equation for the constituent is solved. The dimensionless equations of double-diffusive convection of an incompressible fluid in Boussinesq approximation are:

$$\nabla \cdot \mathbf{u} = 0, \tag{1}$$

$$\frac{1}{\mathrm{Pr}}\left(\frac{\partial \mathbf{u}}{\partial t} + \mathbf{u}\cdot\nabla\mathbf{u}\right) = -\nabla p' + RaT'\mathbf{n} - Ra_C C'\mathbf{n} + \nabla^2\mathbf{u}, \tag{2}$$

$$\frac{\partial T'}{\partial t} + \mathbf{u}\cdot\nabla T' = \nabla^2 T', \tag{3}$$

$$\frac{\partial C'}{\partial t} + \mathbf{u}\cdot\nabla C' = \frac{1}{Le}\nabla^2 C', \tag{4}$$

where p', T', and C' are pressure, temperature, and compositional perturbations respectively, and $\mathbf{u}$ is the velocity vector.

The dynamics of the double-diffusive system is thus governed by four dimensionless parameters: (a) the Rayleigh numbers, which are measures of the driving or restoring forces. The compositional Rayleigh number is $Ra_c = \frac{\beta g \Delta C d^3}{\kappa_T \nu}$, and the thermal $Ra = \frac{\alpha g \Delta T d^3}{\kappa_T \nu}$, where ρ is density, g is gravity, α and β are coefficients of thermal expansion and saline contraction respectively, here taken to be both constant, d is the depth of the layer, κ_T is the thermal diffusivity, ν is the kinematic viscosity or momentum diffusivity. (b) The buoyancy ratio $R_\rho = Ra_c/Ra = \frac{\beta\Delta C}{\alpha\Delta T}$ is the ratio between chemical contribution to the forces to that of thermal contribution; (c) Lewis number $Le = \kappa_T/\kappa_C$, the ratio of thermal diffusivity to chemical diffusivity κ_c, and (d) Prandtl number $\mathrm{Pr} = \nu/\kappa_T$, the ratio of momentum diffusivity to thermal diffusivity.

The numerical code uses the finite volume method on a staggered grid for the spatial discretization (Wong et al., 2022). The face values of the diffusive fluxes are computed with a centered scheme, while the advective fluxes are interpolated using an upwind-biased scheme. The time integration is performed using the Crank-Nicolson method. All the schemes are second-order accurate. We employ a multigrid method (Wesseling, 1992) and the SIMPLE pressure correction algorithm (Patankar, 1980) to efficiently solve the resulting system of equations. A domain-decomposition approach implemented using the Message Passing Interface allows for the parallel execution on distributed-memory systems. The code has been validated by comparing computed critical Rayleigh numbers to the theoretical values determined by a linear stability analysis, by comparing time-averaged Nusselt numbers to published data (Knobloch et al., 1986), and by conducting a comparison with another code on hand (Schmalzl et al., 2002), which was developed to investigate the properties of turbulent convection.

Estimating the thermal Rayleigh number for the subsurface ocean can be a challenge, as the depth and the superadiabatic temperature contrast across the ocean are unknown. One way is to use the scaling relation of Nu $\sim Ra^{\beta}$ where β is some constant (a fraction <1), and assuming a heat flux to infer Ra, which is on the order of $\sim 10^{16}$–10^{22} (e.g., Melosh et al., 2004; Soderlund, 2019). Simulating double-diffusive convection with such Ra would require enormous computing power, and here we test a range of Ra from 10^{8}–10^{11}, to observe the dynamics first with the goal to later extrapolate to high Ra regimes when a theoretical explanation can be constructed with scaling laws. We note that use of eddy viscosities and diffusion coefficients to represent subgrid-scale mixing processes, as is common practice in GCM ocean modeling (e.g., Ashkenazy & Tziperman, 2021), could lower the Ra by orders of magnitude. However, while the eddy viscosity is useful in simulating large-scale cirulcation, it simplifies the small-scale features like salt fingers and plumes in the sublayers that could be changing or limiting the flow and thus the trajectory of double-diffusive evolution. Therefore ultimately extrapolating to the proper dimensionless Ra regime is necessary in future work. Regardless, the range of Ra explored here is prodigious.

The Prandtl number of water can be calculated from the properties of water, which averages at around 7 and can go up to around 10 from the values of terrestrial ocean water depending on the depth and salinity (e.g., Fernando, 1989b; Newman, 1976; Sharqawy et al., 2010; Spigel & Priscu, 1998). Taking $\nu = 9.84 \times 10^{-7}$ m^2/s and $\kappa_T = 1.4 \times 10^{-7}$ m^2/s, Pr ≈ 7. The Lewis number is $\approx$100 with $\kappa_C = 1.1 \times 10^{-9}$ m^2/s. These values of Pr and Le are commonly used in studies of double-diffusive convection (e.g., Krishnamurti, 2009; Radko, 2013).

The buoyancy ratio R_ρ is related to the temperature and compositional distributions, which are uncertain in the subsurface ocean. The in situ measurements of Enceladus' plumes offer clues of the composition of the subsurface ocean, whereas those of the other satellites remain largely speculative. Several factors affect the concentration distribution of the ocean, such as water-rock interaction at the bottom of the ocean, melting and freezing at the interface with the icy shell, as well as external forces from rotation, libration of the icy shells, and tidal effects. Layering occurs in the diffusive regime under subcritical conditions, which means that the restoring forces are greater than the driving forces. Thus the forces due to concentration are greater than those due to temperature, such that R_ρ has to be larger than 1. Vance and Brown (2005) suggested that for an ocean of 100 km with a range of temperature difference $\Delta T = 10^{-4}$ – 10 K, the diffusive regime is possible for $1 \leq R_\rho < 10$, corresponding to concentration (or salinity) difference $\Delta C \sim 1$–10^{-6}. As there are very few exact constraints on the temperature at the bottom of the ocean, we start with this suggested parameter range for R_ρ. We experiment with two values of buoyancy ratio with about half an order of magnitude interval that represent a moderate ($R_\rho = 3$) and large concentration difference ($R_\rho = 10$) between the top and bottom of the ocean, with the bottom being more concentrated.

The influx and outflux of salt alter the evolution of the double-diffusive system. To compare various scenarios of compositional transfer into and out of the subsurface ocean, we apply two simple types of compositional boundary conditions: one is a closed system with no salt fluxes, and the other having a fixed low concentration ($C(z = 0) = 0$) on the top boundary and high concentration on the bottom boundary ($C(z = 1) = 1$) allowing salt fluxes to go in and out. The setting of fixing the concentration at the boundaries simulates the scenario at which salt is replenished at the bottom and lost at the top, possibly due to the dilution by fresh ice melting. The closed system can offer a comparison with a time-changing boundary concentration, since the salt would be transported into the layer and the concentration difference across the layer and thus the buoyancy ratio would change. Thus for systems with chemically insulated boundaries, the R_ρ outlined above would be the initial buoyancy ratio. For the thermal boundary conditions, the temperatures are fixed at the boundaries, set to be cold ($T(z = 0) = 0$) on top and hot ($T(z = 1) = 1$) at the bottom.

In a nonlinear system, the initial condition has an important role in the evolution. When two systems with the same model parameters have slightly different initial stratification, totally different systems will emerge. We model the subsurface water layer in Europa using initial conditions in the diffusive regime: a destabilizing thermal density difference (warm at the bottom, cold on top) and simultaneously a stabilizing compositional (salt) distribution which is heavier at the bottom and lighter on top. Here, we assume two plausible initial temperature conditions: (a) uniformly cold ($T = 0$); (b) uniformly warm ($T = 0.5$) (Figure 2 and Figure S1 in Supporting Information S1, top row). While it is also plausible that the subsurface ocean could have formed from a hot material cooled to its current form, the scenario of uniformly hot ($T = 1$) initial conditions is symmetrical to the uniformly cold conditions, meaning that the solutions to the set of equations would be identical but flipped around the depth of 0.5. This is possible when the concentration and velocity boundary conditions at the top and bottom

are the same and the temperatures are fixed. If a layer was heated up from the bottom by an initially cold ocean and convection starts from the bottom, an initially hot ocean would be cooled down from the top and convection would develop from the top since the temperature of the fluid there is hotter than the boundary temperature. The calculated system properties such as heat flow and r.m.s. velocities should be the same. Therefore here we do not include numerical experiments with high initial temperatures. The initial compositional distribution is a constant gradient which is concentrated at the bottom and dilute on top. The systems are initiated by a slight sinusoidal temperature perturbation.

We model the system in a 2-D box with no-slip mechanical boundaries horizontally and free-slip vertically, and isolating temperature boundaries on the sides. The resolution presents a challenge to simulating a vigorosly convecting double-diffusive system. The interfaces between the layers have to be well-resolved as the property changes there are abrupt. We use a resolution of 1,024 in each dimension for Ra = 10^8 and 10^9, and it is increased to 2,048 for Ra = 10^{10} and 4,096 for Ra = 10^{11}.

4. Results

Depending on the initial conditions, boundary conditions, the buoyancy ratio, and the Rayleigh number, the systems have different outcomes such as well-mixed convection, partial or localized convection, or convection may cease altogether. Table 1 and Figure 1 summarizes the outcomes of the model runs, and their various evolution pathways are described in this section. The description here aims to capture the major events during layer evolution to discuss possible evolution scenarios, while tracking of the detailed properties of the layers such as their temperatures, concentrations, precise layer depths, and their exact duration of existence will be deferred to later studies which will look more closely into the transport through each layer.

4.1. Formation and Merging of Layers

At a lower buoyancy ratio R_ρ = 3, the systems tend to become a well-mixed convecting box after the formation and merging of layers. Figure 2 shows an example of layer evolution of a case starting with low temperatures at a high Rayleigh number. For an initially cold system, a convecting layer quickly develops at the boundary bottom. This first convecting sublayer expands in depth and pushes the conducting part until it becomes unstable and the growth in depth slows down (Figure 2b). The depth of the first sublayer below the conducting part seems to be independent of Ra for Ra $\geq$ 10^9. At a lower Ra = 10^8 with fixed concentration at the boundaries, the first sublayer grows to about 0.7 of layer depth before the conducting part starts to convect. The differences in the temperatures and concentrations between these two layers are continuously reduced, as the later-developed convecting sublayer is further pushed to become a thin conducting sublayer and eventually disappears as the whole system is homogenized. At higher Ra, staircase-like structures first appear above the initial convecting sublayer, while the conducting part continues to thin and more sublayers are developed extending to the boundary (Figure 2c). As the last conducting part becomes unstable and starts to convect, the staircase structures merge into fewer but wider convecting sublayers (Figure 2d), then into two major convecting sublayers (Figure 2e), and then homogenize into a well-mixed layer with temperature and concentration of the bulk part equal to 0.5 except close to the boundaries which are subjected to boundary conditions (Figure 2f).

For the cases with warm initial conditions, the convecting sublayers develop both from the top and the bottom boundary, stretching toward the middle (Figure S1 in Supporting Information S1). In low Ra (10^8), convection ceased in the case with fixed concentration boundaries, which is an exception that will be discussed in a later section. In the cases of Ra = 10^9, the middle conducting sublayer is continually thinned until it becomes unstable when the top and bottom convecting sublayers grow to about 0.4 of the domain depth. It later disappears entirely, leaving two convecting sublayers before finally becoming homogenized. As Ra increases, the evolution of the staircases is even more complex. At Ra = 10^{10}, in the case of fixed concentration boundaries, the initial depth of the convecting sublayers reaches about 0.2 each before instabilities in the middle appear, whereas at Ra = 10^{11} it grows to about 0.3. The staircases first emerge near the interface between the convecting sublayers and the conducting middle part, and then they spread toward the middle, occupying the entire middle sublayer (Figure S1c in Supporting Information S1). The staircases merge forming a convecting sublayer in the middle, which later evolves into a two-layer system and becomes well-mixed. As noted in the Methods section, due to the symmetry

Table 1
Results of the Model Runs

Ra	R_ρ	IC[a]	BC[a]	Outcome[a]	Time of merging	Remarks[b]
10^8	3	Cold	No flux	a	0.367	
10^8	3	Warm	No flux	a	0.318	
10^8	3	Cold	Fixed C	a	1.26	
10^8	3	Warm	Fixed C	b		
10^8	10	Cold	No flux	b		
10^8	10	Warm	No flux	b		
10^8	10	Cold	Fixed C	b		
10^8	10	Warm	Fixed C	b		
10^9	3	Cold	No flux	a	0.0879	Figures 7 and 8
10^9	3	Warm	No flux	a	0.144	Figure 7
10^9	3	Cold	Fixed C	a	0.191	Figures 6 and 7
10^9	3	Warm	Fixed C	a	0.301	Figures 6 and 7
10^9	10	Cold	No flux	a	1.63	Figure 8
10^9	10	Warm	No flux	b		
10^9	10	Cold	Fixed C	b		
10^9	10	Warm	Fixed C	b		
10^{10}	3	Cold	No flux	a	0.03	Figures 7 and 8
10^{10}	3	Warm	No flux	a	0.0816	Figures 7 and 8
10^{10}	3	Cold	Fixed C	a	0.0471	Figures 6 and 7
10^{10}	3	Warm	Fixed C	a	0.134	Figures 6 and 7
10^{10}	10	Cold	No flux	a	1.0	Figure 8
10^{10}	10	Warm	No flux	a	0.84	Figure 8
10^{10}	10	Cold	Fixed C	c		Figure 4
10^{10}	10	Warm	Fixed C	b		
10^{11}	3	Cold	No flux	a	0.0146	Figure 7
10^{11}	3	Warm	No flux	a	0.019	Figure 7
10^{11}	3	Cold	Fixed C	a	0.0223	Figures 2, 3, 5, 6, and 7
10^{11}	3	Warm	Fixed C	a	0.0348	Figure 3, Figures 1 and 2 in Supporting Information S1
10^{11}	10	Cold	No flux	c		
10^{11}	10	Warm	No flux	c		
10^{11}	10	Cold	Fixed C	c		Figure 4, Figures 3 and 4 in Supporting Information S1
10^{11}	10	Warm	Fixed C	c		Figure 4, Figures 5 and 6 in Supporting Information S1

[a]References for outcomes: a - layers eventually merged; b - convection ceased; c - one or more convecting sublayers lasting for a dimensionless time $O(10^{-1})$ for $Ra = 10^{11}$ and O(1) for $Ra = 10^{10}$. IC, initial conditions; BC, boundary conditions. [b]The cases illustrated in the figures are flagged under remarks.

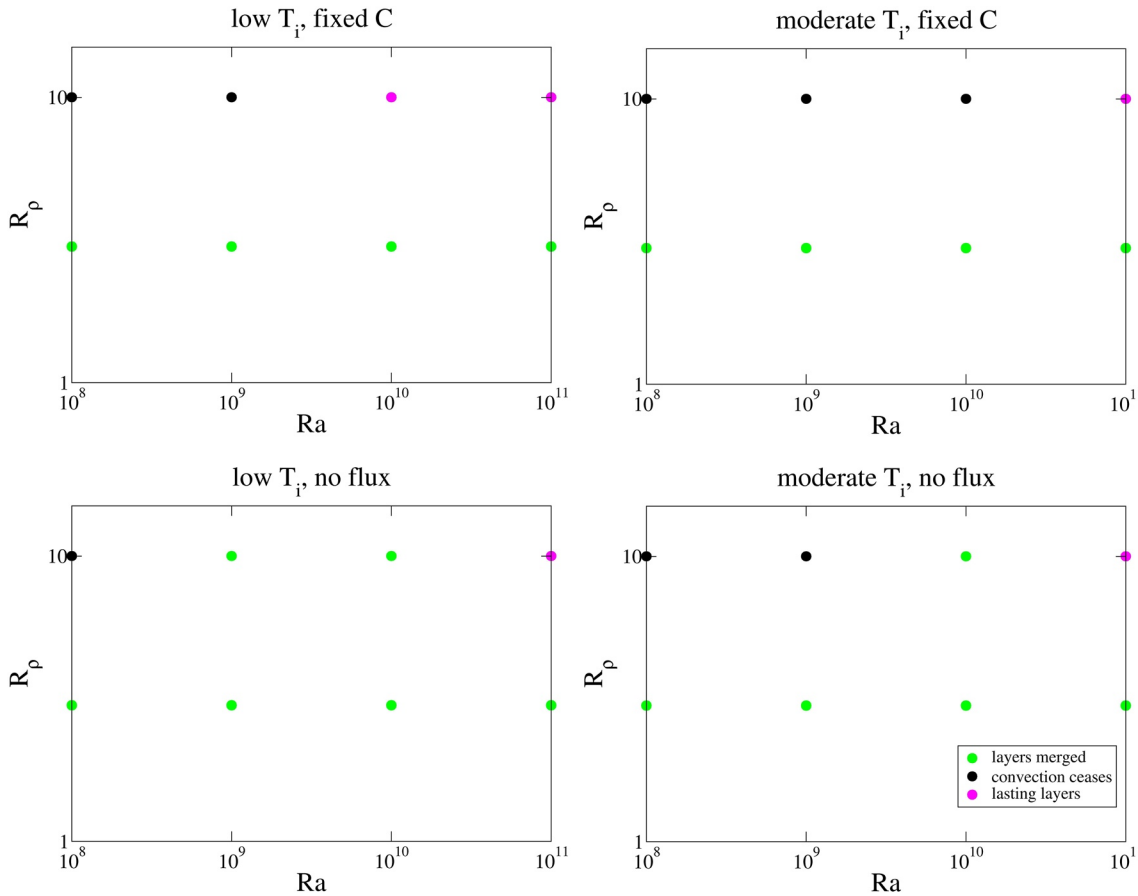

Figure 1. Outcomes of model runs with respect to Ra and R_ρ, with different initial conditions and boundary conditions.

of the setup, the evolution of a system initiated with high temperatures would be the same as that with low temperatures but inverted top and bottom.

While the sublayers exist, the flow of material is limited to within the sublayers, as clearly demonstrated in Figure 3. The sublayers, which are self-organized by the dynamics of the flow rather than by any a priori ad hoc formulated boundaries, are very effective at separating material in each individual sublayer. Material from greater depth would not show up at the surface, since the boundaries between the sublayers would hardly allow any advective transport across them. This can be shown by the evolution of different blocks of passive tracer particles, injected in the layers at a given time step. Mixing occurs within each sublayer so that the layers have distinct concentrations and temperatures. This shows that the ocean could maintain a well structured interior rather than being thoroughly mixed. The materials from the bottom are prevented from reaching the surface, thus the surface features might not reflect the composition of the materials at depths.

When the boundary conditions are changed, the thicknesses of the individual sublayers are different. When no concentration fluxes are allowed on the boundaries, the depths of the first sublayer before another sublayers develops are slightly larger. The largest effect of chemically insulated boundaries is on the persistence of layers, as the evolution sequence is accelerated and mixing occurs in a shorter time.

4.2. Partial Convection and Cessation of Convection

The occurrence of convection becomes less likely, although not entirely impossible, when the restoring forces are enhanced with a higher buoyancy ratio.

As the buoyancy ratio is increased to $R_\rho = 10$, the restoring force is increased and the systems tend to evolve to a more stable state, whether it be partially convecting, or not convecting at all. The boundary conditions play a more

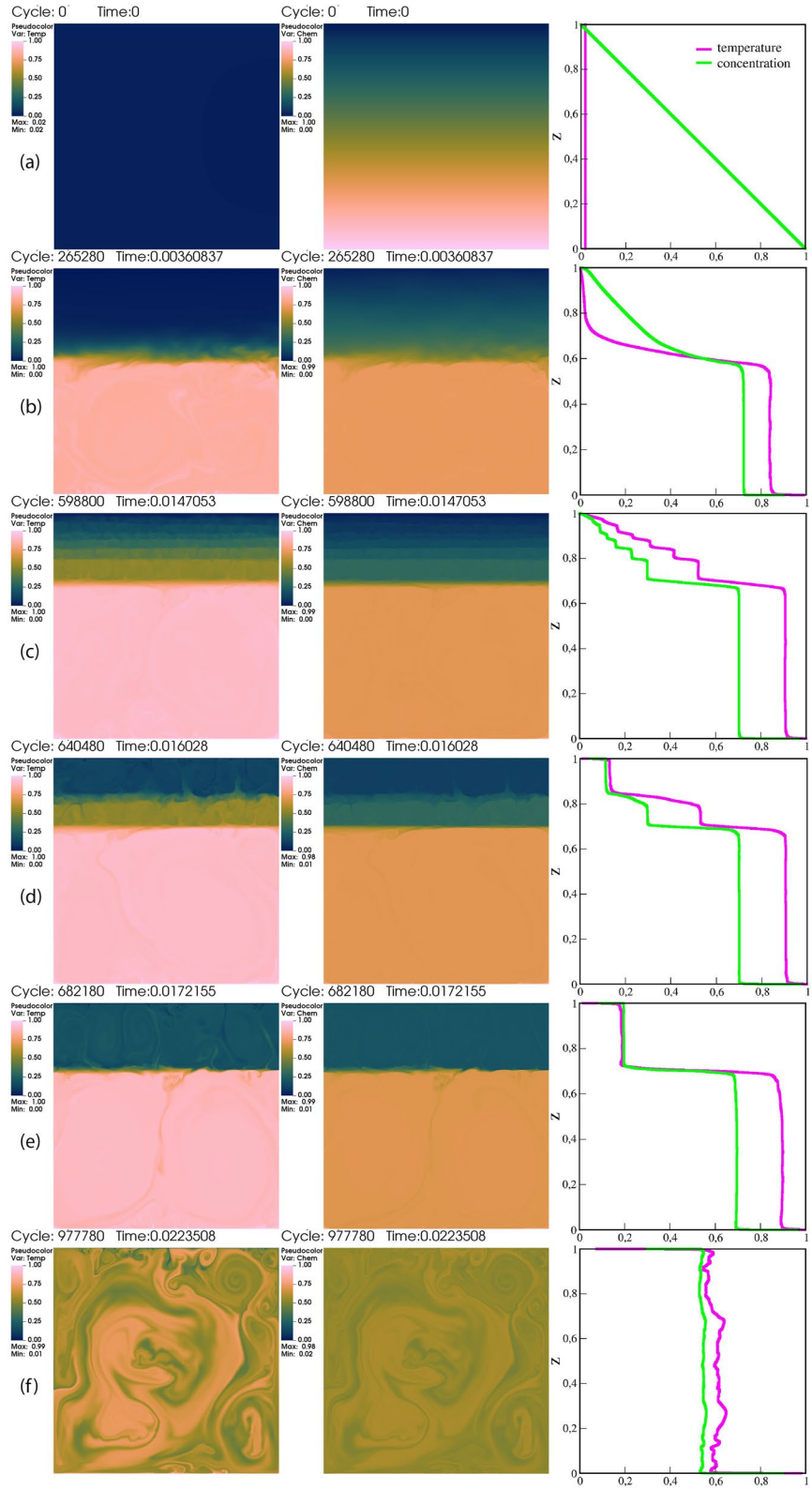

Figure 2. Snapshots of temperature, composition, and their horizontally averaged profiles at various time points, for a case with Ra = 10^{11}, $R_\rho = 3$, starting with a low initial temperature. The concentration is fixed at the boundaries ($C = 0$ on top, 1 at the bottom).

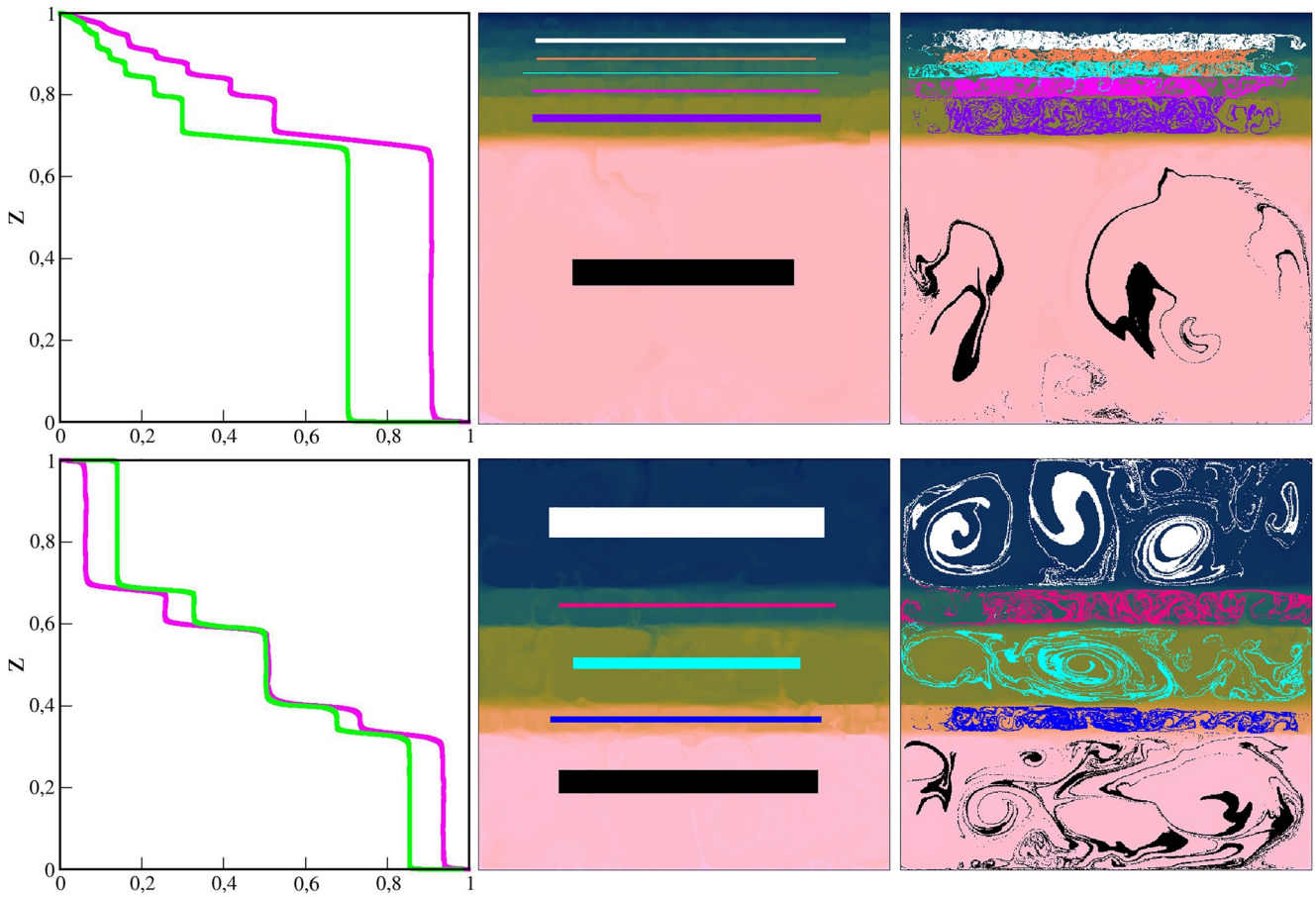

Figure 3. Snapshots of developing layers illuminated with tracers, and their corresponding profiles of temperatures and concentrations (left, red curve is temperature and green is concentration). 10^5 tracers of contrasting colors against the colors of the temperature field are initially placed within each sublayer as rectangular boxes (middle column), and after a short while the tracers are distributed as shown in the right column, displaying flow patterns. The top row shows the case Ra = 10^{11}, $R_\rho = 3$, starting with low temperatures, and bottom row shows the same case with medium initial temperatures.

decisive role in the occurrence of convection. Maintaining the concentration difference reinforces the chemical contribution to the restoring buoyancy force, which helps stabilize the system and prevent it from convecting.

Since the restoring force is greater at this buoyancy ratio, a higher Ra is required to prevent convection from ceasing, as Ra = 10^8 is not sufficient to have convection and the system is quickly stabilized to a conducting layer. At Ra = 10^9, in the case with fixed concentration boundaries, the system is also quickly stabilized and convection ceases, whereas in the cases with no-flux boundaries convection continues on and the system is eventually homogenized. In the cases with low initial temperatures, the convecting sublayer in these cases grows to more than 0.4 of the layer depth before the rest of the system starts to convect, and the two-layer convecting system eventually merges and becomes well-mixed. However, when the system starts with a medium temperature, convection ceases regardless of boundary conditions. This warm initial condition might also be another reason (besides the boundary condition) for the exception in the case of $R_\rho = 3$ and Ra = 10^8 with fixed concentration boundaries, in which convection ceases instead of the system being homogenized.

Various outcomes are observed as Ra is increased to 10^{10}. Convection can occur partially, and some systems can even reach a well-mixed state, or convection may also cease. In systems with low initial temperatures and fixed concentration, the convecting sublayer develops from the boundary, continues to grow slowly as it reaches about ∼0.2 of the depth (Figure 4 left). In the cases where no chemical fluxes are allowed through boundaries, the growth of this bottom convecting sublayer is much faster and later the sublayers merge to become a homogenized system. Cases with a medium initial temperature see different outcomes with different boundary conditions as well. Convecting sublayers first develop from both the top and bottom boundaries in the case with no-flux

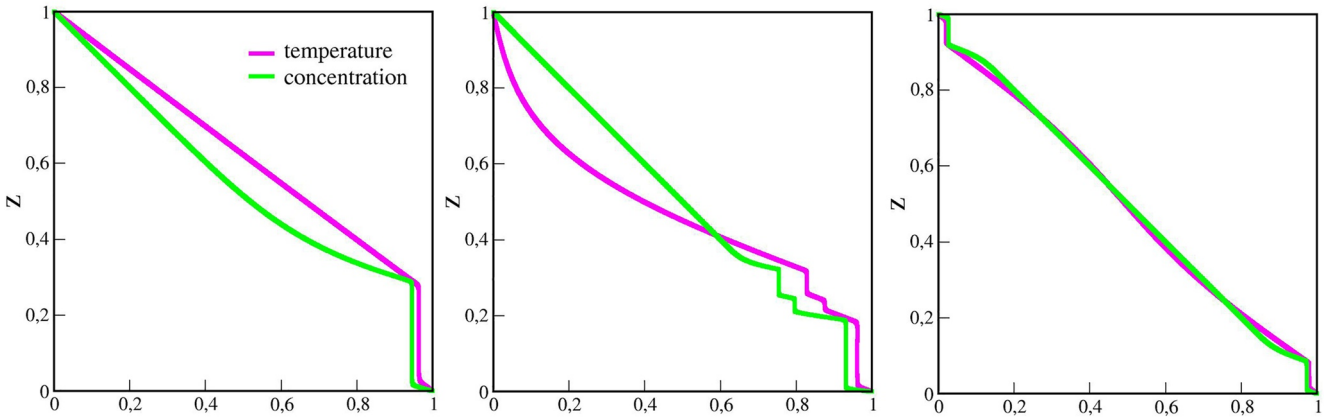

Figure 4. The convecting sublayers emerge from the boundaries in cases with $R_\rho = 10$ and fixed concentration boundaries. Left figure shows case Ra = 10^{10}, initially cold; middle figure Ra = 10^{11}, initially cold; and right figure Ra = 10^{11}, initially warm. When the system is heated up from the bottom in the case starting with low temperatures (left, middle), the initial convecting sublayer grows from the bottom to a certain depth and then it thickens very slowly, and in the case of high Ra staircases can be seen above the bottom convection sublayer. In the initially warm case (right), convection develops from both top and bottom, and the depth of these convecting layers are able to remain stable at this Ra.

boundaries and later merge and become well-mixed, whereas convection ceases if the boundaries have fixed concentration.

In high Ra cases (Ra = 10^{11}), partial convection occurs in all cases. In the systems initialized by a uniformly low temperature with fixed concentration boundaries, after the initial convecting sublayer develops, staircases appear near the interface between this convective sublayer and the conductive layer (Figure 4 middle, Figure S3 in Supporting Information S1). The staircases later begin to merge, with the step in temperature merging first before that in concentration (Figure S3e in Supporting Information S1). The remaining 2 convecting sublayers continue to grow in depth, and the temperature and concentration of the middle sublayer gradually increase to be closer to that of the bottom convective sublayer (Figure S3f in Supporting Information S1). While the thickness, temperature, and concentration of convecting sublayers remain the same in this stage, the temperature gradient in the non-convecting part, which is initially increasing, approaches a constant (Figures 3e and 3f in Supporting Information S1). The evolution of the equivalent case with no-flux boundaries is similar, with these stages proceeding at faster pace than in the system with fixed concentration boundaries, and having a thicker and less concentrated convecting bottom sublayer as the concentration at the bottom boundary is not kept constant.

The case starting with medium temperature and with fixed concentration boundaries has convecting sublayers on both the top and the bottom, and a middle sublayer develops with almost constant gradients in temperature and concentration without staircases (Figure 4 right, and Figure S5 in Supporting Information S1). Both the top and the bottom convecting sublayers remain at ~0.08 in depth for a long period, while the heat flow and velocities seem to be statistically steady (Figure S6 in Supporting Information S1), leading one to speculate that they may be long-term stable structures. In the case with no-flux boundaries, however, the top and bottom convecting layers continue to grow slowly as the concentrations in these layers go toward the average.

5. Lifetime of Layers

In the cases where convecting sublayers emerge, the duration of their existence varies with the initial conditions, boundary conditions, and buoyancy ratio as described in the previous section. This section explores how much the timing is influenced by various factors.

The evolution of the system can be tracked by the change in heat flow and r.m.s. velocity. The heat flow is represented by the Nusselt number Nu = $dF/k\Delta T$ (k is the thermal conductivity, F is the heat flux), which is the ratio of total heat flux by convection and conduction to the theoretical conductive heat flux in the absence of convection. An example is shown in Figure 5, of the case in Figure 2. The heat flow is statistically steady during the formation of staircases and sublayers, and its magnitude depends on the number of sublayers present in the system. As the remaining conducting part becomes unstable, the heat flow and the velocity begin to rise. When this part becomes

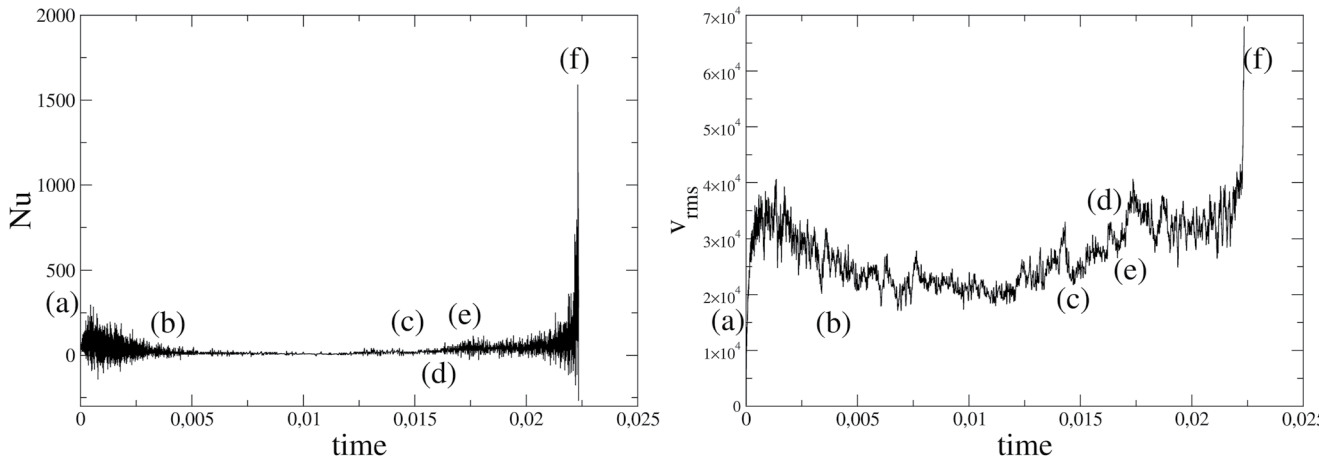

Figure 5. The heat flow (nondimensional, Nusselt number) and r.m.s. velocity of the system in Figure 2, Ra = 10^{11}, $R_\rho = 3$, initially cold, and with fixed concentration boundaries. The letters refer to the stages labeled in Figure 2.

a convecting sublayer, the heat flux and the r.m.s. velocity both have a several-fold increase, and the fluctuation in heat flux becomes significantly larger (Figures 6 and 7). The heat flux and velocities climb further as more convecting sublayers are thinned out and disappear, resulting in a 2-layer system, and eventually, when all the layers are mixed up the heat flow surges. The evolution is even more pronounced in some cases with warm initial temperatures, as the 3-layer stage lasts longer before the middle layer is narrowed and disappears. The Nusselt number during the stage of developing layers in warm start cases is also slightly smaller, due to the presence of convecting layers emerging from both top and bottom boundaries. The simulations are terminated when the system becomes completely well-mixed, or when the heat flux is statistically steady. In the well-mixed case, as the temperature and concentration are now in phase, the system is symmetric around mid-depth and it would not change its state unless something asymmetric occurs (such as on the boundaries, which is not considered here).

While we do not stress absolute times here, the dimensionless times shown can be scaled by d^2/κ_T, which for Europa ($d \sim 100$ km) = 2×10^9 yr. So dimensionless times of O(10^{-1}) to O(1) in Table 1 could imply substantial portions of geologic time and even when extrapolated to higher Ra.

5.1. Initial Conditions

In most cases where merging occurs, warm initial conditions can prolong the time of merging from about 20% longer to more than twice as long (Figure 6). This might be due to the number of convecting sublayers, because under warm conditions convection these can develop from both the top and the bottom, and the stage with 3 convecting sublayers, which is absent in cold initial conditions, takes longer to merge. There are exceptions in the cases where convection ceased with warm initial conditions under fixed concentration boundary conditions and low Ra (10^8), or when the buoyancy ratio $R_\rho = 10$ in a low Rayleigh number (Ra = 10^9) scenario even when no fluxes are allowed into the system (see Table 1). Another exception is in a high R_ρ and Ra = 10^{10} scenario with no-flux boundaries, when the medium initial temperature case merges faster than the low initial temperature cases. One explanation could be that warm initial conditions favor a steady state, especially under the influence of a larger restoring force, whether the system is ceasing convection or becoming well-mixed.

The initial conditions require knowledge of the primordial subsurface ocean. For example, the primordial subsurface ocean could have been formed at the same time as the moon itself, in which case the initial ocean could be hot or warm; or it could have remelted from frozen ice heated by tidal or radioactive sources (e.g., Nimmo & Pappalardo, 2016), and the ocean would be formed cold. Such conditions may be obtained later, as thermal conditions may have varied as ice shell thickness waxed and waned (Hussmann & Spohn, 2004). Recent studies have stressed the importance of salinity variations over those of temperature for Europa's ocean (e.g., Ashkenazy & Tziperman, 2021), increasing the potential importance of ocean stratification and double-diffusive convection. While salinity variations due to freeze/thaw at the ocean/ice-shell boundary have been incorporated in such

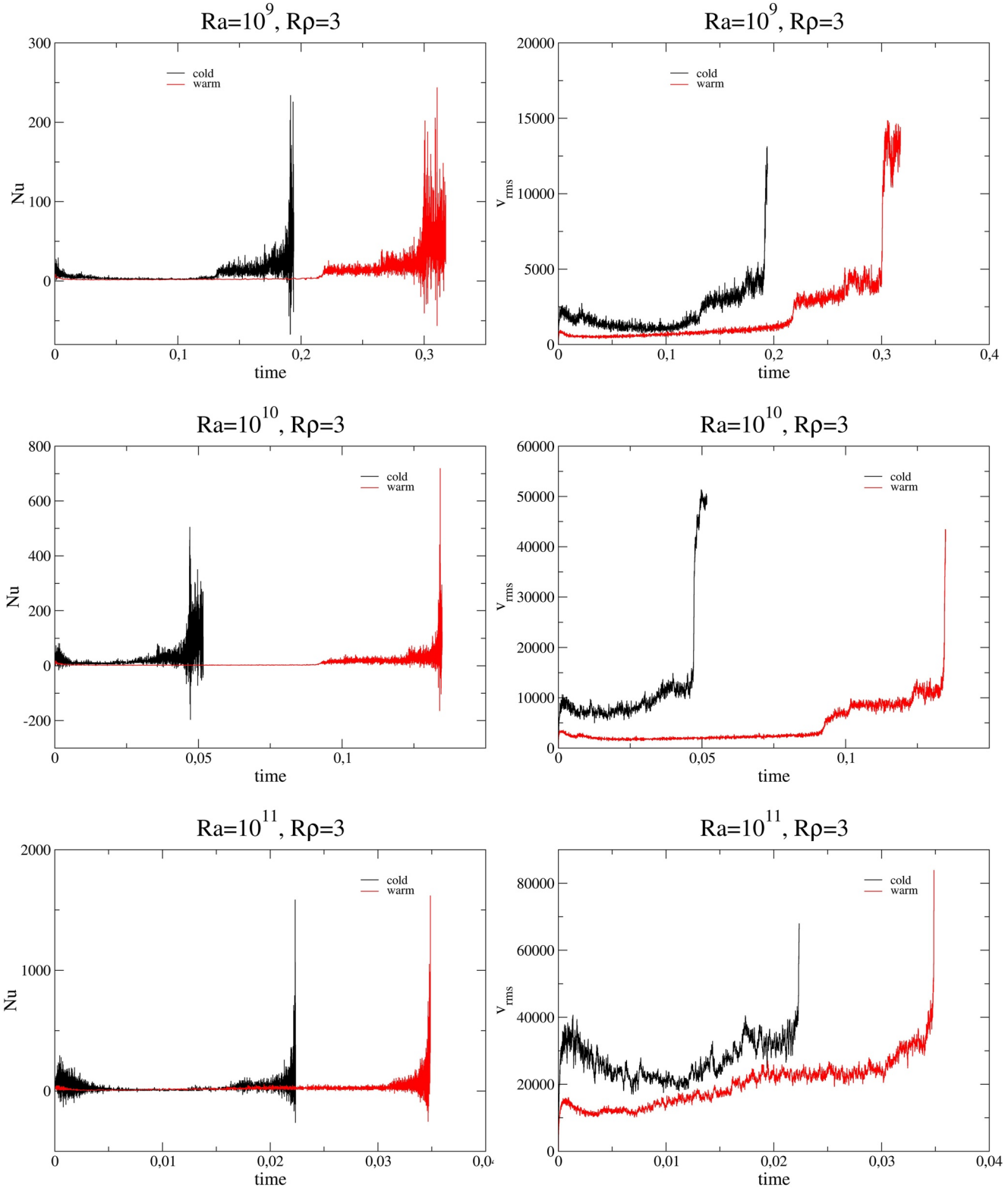

Figure 6. Time evolution of heat flow (Nu, non-dimensional) and r.m.s. velocities with different initial conditions and fixed boundary concentrations throughout the numerical running time.

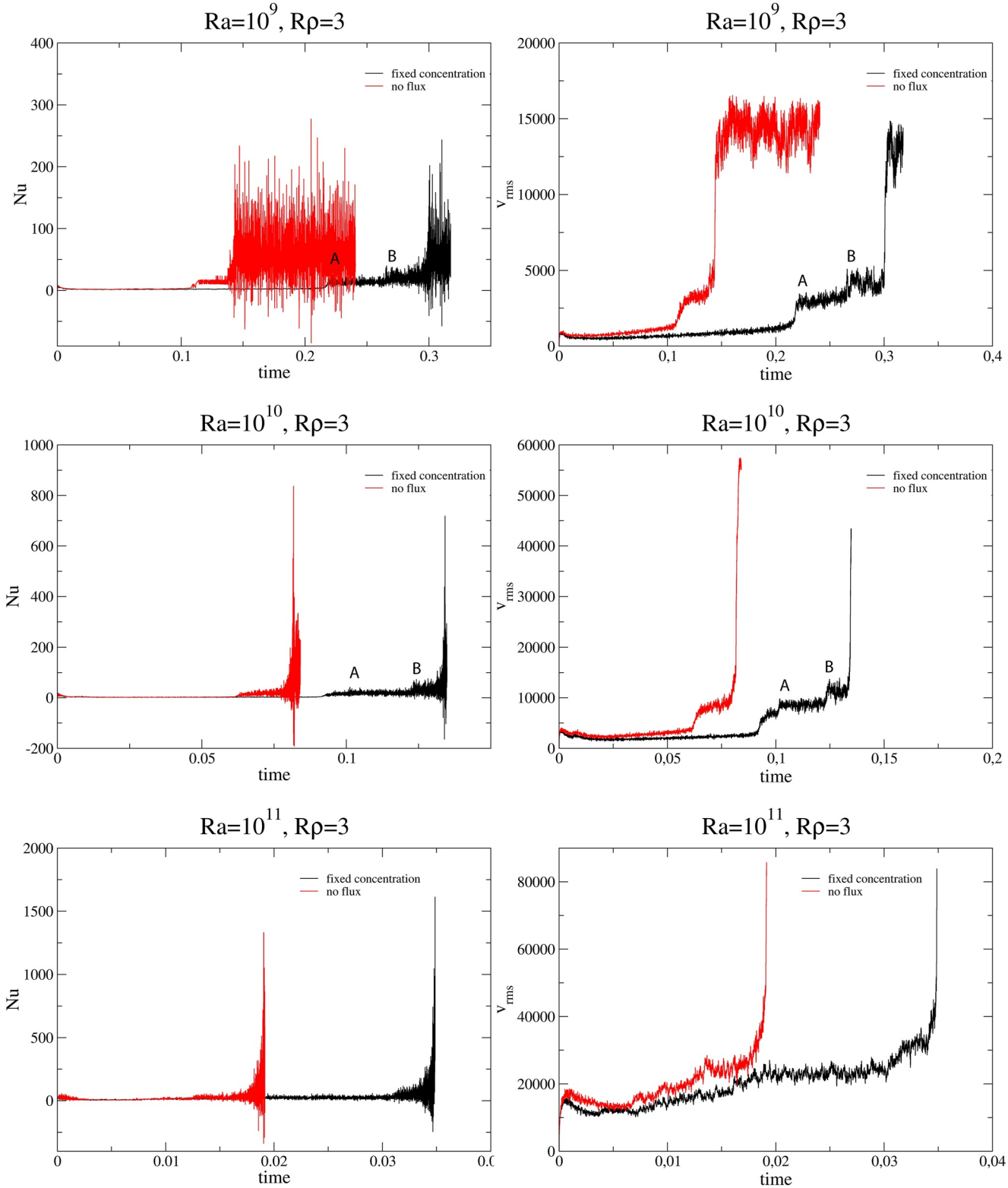

Figure 7. Comparison of the evolution of systems with different concentration boundary conditions for a case with Ra = 10^{10}, $R_\rho = 3$, starting with a medium initial temperature. The increase in Nu and velocities as the staircases merged to 3 layers (labeled A) and 2 layers (labeled B) are marked for the cases with fixed concentration boundaries (black curve).

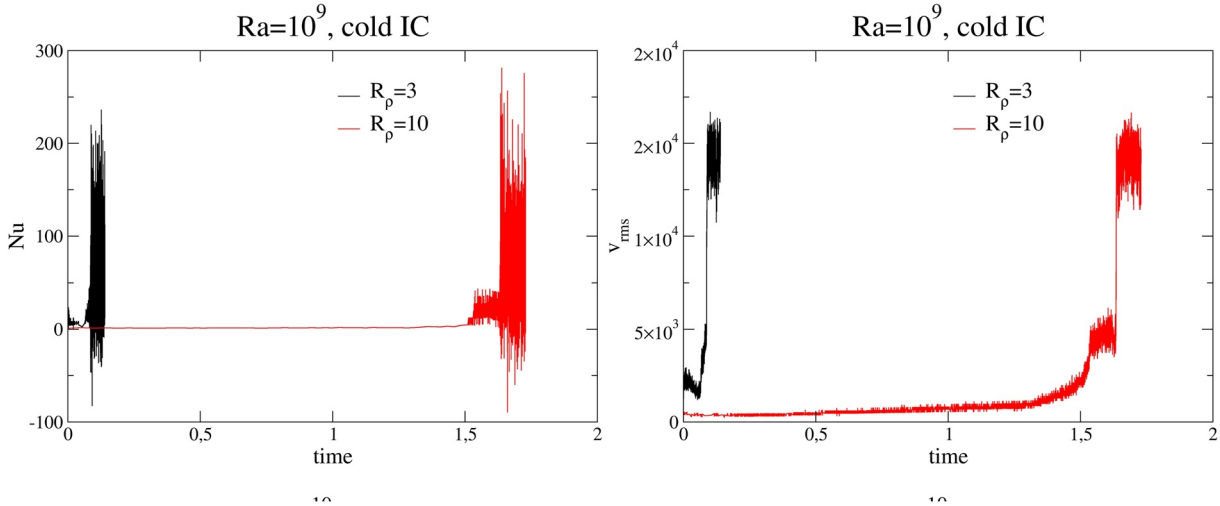

Figure 8. Comparison of the evolution of systems with different buoyancy ratios R_ρ with no flux boundaries.

models, greater attention to possible saline fluxing through the seafloor, and indeed, the creation and history of ocean salinity may prove equally relevant.

5.2. Boundary Conditions

Fixing the concentration at the boundaries has the effect of maintaining the concentration difference across the layer, such that the stabilizing force is sustained. When the concentration of the boundaries is fixed, the systems have a longer stage where the sublayers develop, and also a longer stage with 2 or 3 major convecting layers when compared with cases where no chemical fluxes are allowed. This can be seen clearly in the increase in velocities (Figure 7). The time before the layers merge is also ∼50% to more than twice as long as the cases with no fluxes across the boundaries.

While the boundary conditions here are highly simplified as constant spatially and in some cases temporally, in reality they are subjected to the properties of the ice-water and water-rock interfaces and changes in the heat transfer processes in the silicate interior and the icy shell (e.g., Behounková et al., 2021; Buffo et al., 2021; Cadek et al., 2019; Zhu et al., 2017). The idealized models here may represent part of the subsurface ocean, and layering may not be a global phenomenon, as in the Earth's ocean. If forced boundary conditions, that is, specified compositional gradients dC/dz are applied at the boundaries, possibly to mimic melt water or chemical reactions at the interface, the lifetime may change as well. As the dynamics of the ocean could be greatly altered by the boundaries, further studies will have to include the solidifying and melting processes at the interfaces, and this may involve coupling with the evolution of the icy shell and the silicate interior.

5.3. Buoyancy Ratio

A higher buoyancy ratio enhances the restoring force and can significantly increase the lifetime of layers as the stabilizing force is much stronger. A increase of R_ρ from 3 to 10 can lead to ∼30 times longer duration of layer existence (Figure 8).

The Nusselt number is also significantly reduced at $R_\rho = 10$. At $R_\rho = 3$, while the values of Nu vary with Ra and can be more than 10 in the presence of multiple layers, Nu in the cases with $R_\rho = 10$ is slightly larger than 1, indicating that heat transport is very inefficient as a large part of the layer is not convecting.

As the composition distribution of the oceans in question are unclear, whether the concentration difference for R_ρ to be 10 could be reached in subsurface oceans conditions is yet to be evaluated. Taking the values of seawater as reference, for a temperature difference ranging from $\Delta T = 10^{-4}$–10^{1} K, the saline contraction coefficient $\beta = 0.8\ \mathrm{g}^{-1}\ \mathrm{kg}$, and a thermal expansion coefficient $\alpha = 2 \times 10^{-5}\ \mathrm{K}^{-1}$ for saline water at close to 273 K, the smallest concentration difference ΔC required would be 3.25 g kg^{-1} (∼10% of terrestrial water). The measurements

of Enceladus' plume give the concentration of sodium-rich material in the range of 5–20 g kg^{-1} (Postberg et al., 2009) as a lower limit. Such a concentration difference over the depth of its ocean would not be difficult to achieve, and such concentrations have been shown to be possible in modeled compositions of Enceladus' subsurface ocean (e.g., Ingersoll & Nakajima, 2016; Zolotov, 2007). For aqueous $MgSO_4$, referencing the values from Vance and Brown (2005), with $\alpha = 2 \times 10^{-4}$ K^{-1}, $\beta = 0.1$ mol^{-1}, the largest ΔC required would be 0.1 mol or 12 g kg^{-1}. Of course, at low enough salinities and/or pressures, ocean water will exhibit an anomalous thermal expansion, a point returned to below.

6. Discussion of Fundamentals

Our simulations demonstrate that layers can emerge through double-diffusive convection in icy worlds oceans, and while they exist the heat flow is strongly diminished. A partially convecting ocean, where the transport of heat and materials is limited, can develop when the bottom is much more concentrated in salts than the top and the concentration difference is maintained. Under certain circumstances, for example, in the case starting with medium initial temperature, under large concentration contrast ($R_\rho = 10$) and convecting vigorosly ($Ra = 10^{11}$), layers seem to be stable. Are these conditions possible in the subsurface oceans of icy moons? And if so, what does it mean for the thermal history of the icy moons? Understanding the phenomenon of layering is paramount to understanding the evolution of the icy bodies, as layering hinders transport and thus the assumptions of parameterization in evolution models will have to be examined.

An important question is how long can these layers last. As shown in the cases in this study, layers are transient and their longevity depends on various factors. The heat flux fluctuation could increase from two to several fold when each sublayer merges, and the merging of the final sublayers results in a surge in heat and material fluxes (Figures 5–8, Figure S2 in Supporting Information S1). A jump in heat flux could lead to thinning or melting in the ice shell, and the surge as the system becomes well-mixed could be the cause of a possible catastrophic event or global melting in Europa's evolution. Our simulations are non-dimensionalized, and the timescale depends on the depth of the ocean. Yet a critical question is whether the evolution of layers is sensitive to the global depth of the ocean, or if layer growth timescale is a local property that is independent of the entire depth of the ocean. The dynamics of the growth of the initial layers as the system is heated from the bottom or cooled from the top boundaries depends on the local stratification and thermal buoyancy, but not the depth of the entire fluid system, if this global depth is sufficiently deep to render the boundary dynamically unimportant. The lengthscale and thermal diffusion timescale taken from the global depth become relevant when the layering dynamics has advanced to a lengthscale comparable to the depth of the fluid system, which is when layering breaks down to one remaining convecting layer.

We submit that the more appropriate lengthscale for layering dynamics is the local Ra, which is the Ra of individual sublayers. There is existing literature on the parameterization of fluxes through the individual sublayers with the local Ra (e.g., Radko et al., 2014; Turner, 1965; Turner, 1967; Yang et al., 2020), but there are remaining questions for the dynamics of layering: What is the relationship between the first sublayer and subsequent sublayers? How do they emerge and later merge or decay? Are there conditions in which the fluxes into and out of a sublayer are in equilibrium so that the sublayer can last longer? How many layers can develop in the double-diffusive system? What are the depths of the layers? If the flow depends on the size of sublayers, then perhaps it would be useful to develop a model of layer growth and merging in 1-D, for example, relating the fluxes of the layers to larger scaling dynamics (e.g., Radko et al., 2014). Such theoretical models can identify the physical properties that affect the layer evolution. These questions also constitute a fundamentally new aspect of layer growth and merging in double-diffusive research. Before we further elaborate on the timescale on the icy moons, or extrapolate the results to higher global Ra, the problem of how individual layers develop and merge should be addressed.

Finally, rotation can certainly influence, if not dominate, the dynamics in subsurface oceans (e.g., Kelley, 1987; King et al., 2009; Pearlstein, 1981; Soderlund et al., 2014; Stellmach et al., 2014). Rotation weakens convection and inhibits the formation of layers, and various studies have been devoted to exploring regimes where rotation or double-diffusion dominate, and the scaling laws of properties such as heat flux and thicknesses of boundary layers in these regimes (e.g., Carpenter & Timmermans, 2014; King et al., 2013; Liang et al., 2021; Moll & Garaud, 2016; Monville et al., 2019). In a study of rotational convection applied to icy bodies, Soderlund (2019) suggested that the subsurface oceans of Europa, Titan, and Ganymede might belong to a regime where rotational effects are limited, whereas they are more significant on Enceladus. Convection under rotation is currently an area

of active research, and double-diffusive flow under rotation is a complex phenomenon which will be deferred to future studies.

7. Implications on the Structure and Evolution of Icy Moons

In this study, we have demonstrated that layering in the subsurface oceans of icy worlds (outer solar system satellites and Kuiper belt objects) is possible, and the lifetime can be prolonged when a large concentration difference across the ocean is maintained. The transient nature of layers is reflected in the intermittent surges in heat flux as layers merge, which may thin the ice shell and potentially leave its geological imprint on the surface if the ice shell is sufficiently weakened.

We note that while we kept the thermal expansion at a constant value for water in our simulations because the density changes are assumed to be small, but its sign could change with concentration. At temperatures close to 273 K and low salinity, the thermal expansion coefficient α is negative, meaning that the water close to the top of the ocean may be even less dense and thus more stable, further hindering the transport of materials from the bottom. For seawater composition, the anomalous density behavior is eliminated for pressures $\geq$27 MPa (achieved for ice shell $\gtrsim$22 km on Europa) and salinities $\geq$25 g kg^{-1}, so the results presented here refer to such conditions, or more generally, to oceans below any thin, conductive "stratosphere" as proposed by Melosh et al. (2004). With a sign change of thermal expansion, the temperature becomes the stabilizing force. If salts in this top part are distributed such that the concentration provides a small driving force, this layer could be in the finger regime. We note that the conductivity of the ocean inferred from Galileo magnetometer data implies at least a brackish ocean (see discussion on Khurana et al., 2009).

While this study concerns the subsurface oceans of Europa and Enceladus, this setting is applicable to the deeper interior of large icy satellites such as Ganymede and Titan (whose oceans are nominally are sandwiched between the surface ice-I shell and deeper layers of high-pressure water-ice phases). The properties of water such as density, specific heat capacity, and conductivity in the pressure range of the interior in these icy bodies varies by some 10% (e.g., Journaux et al., 2020). As these physical properties are grouped into non-dimensional ratios that characterize the fluid system, their variations are in the same order of magnitude. Needless to say, the effects of the variation in thermal expansivity on temperature, concentration and pressure should be investigated for the oceans in such high-pressure interiors.

The magnetometers on ESA's JUpiter ICy moons Explorer (JUICE) and NASA's Europa Clipper are expected to provide further information on the thickness, salinity, and circulation of the ocean. The magnetic induction response is sensitive to the temperature, pressure, speciation of salt, concentration distribution, and motion in the ocean among other factors, which will affect the electrical conductivity and thus the amplitudes of induction response (Khurana et al., 2009; Vance et al., 2021). Vance et al. (2021) calculated the induced magnetic field strength from a rotating ocean circulation and demonstrated how flow velocities can, in principle, be reflected in such measurements. With multiple flybys of the Clipper and JUICE covering different areas of Europa, Callisto, and Ganymede, the spatial variation in signal strength may reveal the ocean flows, or potentially, a lack thereof. Whether structures such as layering can be identified from magnetic signals is not clear, but their effects conductivity inversions should be assessed.

Future geophysical data, from Europa Clipper and JUICE missions, will further constrain the interior structures of the icy Galilean satellites. The REASON ice penetrating radar can help determine the depth of Europa's icy shell, the occurrence of solid-state convection and thus convective flow patterns in the ice shell, and the extent of the subsurface ocean. The magnetic induction response from the magnetometer would give estimates of ocean salinity and thickness. The imaging and mass spectrometers will further characterize the composition and chemistry on the surface, constraining the identity and possible concentration of salts in the interior. The JUICE spacecraft, which will be probing Callisto, Europa, and especially Ganymede, carries a laser altimeter for topographic measurements, and Doppler tracking to obtain gravity measurements. This data, and the geodetic constraints and Doppler tracking from Clipper, will inform us about the shape of the moons and further confirm the existence of subsurface oceans. Information on the thickness of Europa's ocean should give improved constraints on the ocean convection models described here and the relevant timescales. Gravity data from both JUICE and Europa Clipper can also help determine the seafloor topography or possible lateral compositional heterogeneity in the top part of the silicate interior (Koh et al., 2022), aiding in the characterization of bottom boundary conditions.

Fundamentally, once data is in hand from multiple instruments near and over Europa, we will have a much better constrained picture of this satellite's ocean thickness and composition (salinity), which along with further theoretical and modeling advances, should allow us to test whether layered ocean convection is occurring with Europa today, or whether it perhaps left its imprint/pattern in Europa's surface in the geological past due to heat flow excursions accompanying convective transitions.

Data Availability Statement

The numerical code and the input parameters used in the study are described in detail in the methods and results sections. This source code, input files, and documentation can be found in the repository (Wong et al., 2022).

Acknowledgments
T. Wong acknowledges support from DFG Grant WO 2324/2-1. W. B. M. is supported by NASA's *Europa Clipper* project. The authors are grateful to Carmen Sanchez-Valles, Stephan Stellmach, Kelsi Singer, and Sabine Dude for meaningful discussions. The manuscript has greatly benefited from comments by two anonymous reviewers and the editor Laurent Montesi. Open Access funding enabled and organized by Projekt DEAL.

References

Amit, H., Choblet, G., Tobie, G., Terra-Nova, F., Čadek, O., & Bouffard, M. (2020). Cooling patterns in rotating thin spherical shells—Application to Titan's subsurface ocean. *Icarus*, *338*, 113509. https://doi.org/10.1016/j.icarus.2019.113509

Ashkenazy, Y., & Tziperman, E. (2021). Dynamic Europa Ocean shows transient Taylor columns and convection driven by ice melting and salinity. *Nature Communications*, *12*(6376), 6376. https://doi.org/10.1038/s41467-021-26710-0

Behounková, M., Tobie, G., Choblet, G., Kervazo, M., Melwani Daswani, M., Dumoulin, C., & Vance, S. D. (2021). Tidally induced magmatic pulses on the oceanic floor of Jupiter's moon Europa. *Geophysical Research Letters*, *48*(3), e2020GL090077. https://doi.org/10.1029/2020GL090077

Bire, S., Kang, W., Ramadhan, A., Campin, J.-M., & Marshall, J. (2022). Exploring ocean circulation on icy moons heated from below. *Journal of Geophysical Research: Planets*, *127*(3), e2021JE007025. https://doi.org/10.1029/2021JE007025

Buffo, J., Schmidt, B., Huber, C., & Meyer, C. (2021). Characterizing the ice-ocean interface of icy worlds: A theoretical approach. *Icarus*, *360*, 114318. https://doi.org/10.1016/j.icarus.2021.114318

Cadek, O., Soucek, O., Behounková, M., Choblet, G., Tobie, G., & Hron, J. (2019). Long-term stability of Enceladus' uneven ice shell. *Icarus*, *319*, 476–484. https://doi.org/10.1016/j.icarus.2018.10.003

Carpenter, J. R., & Timmermans, M.-L. (2014). Does rotation influence double-diffusive fluxes in polar oceans? *Journal of Physical Oceanography*, *44*(1), 289–296. https://doi.org/10.1175/JPO-D-13-098.1

Fernando, H. J. S. (1989a). Buoyancy transfer across a diffusive interface. *Journal of Fluid Mechanics*, *209*, 1–34. https://doi.org/10.1017/S0022112089003010

Fernando, H. J. S. (1989b). Oceanographic implications of laboratory experiments on diffusive interfaces. *Journal of Physical Oceanography*, *19*(11), 1707–1715. https://doi.org/10.1175/1520-0485(1989)019<1707:OIOLEO>2.0.CO;2

Goodman, J. C., Collins, G. C., Marshall, J., & Pierrehumbert, R. T. (2004). Hydrothermal plume dynamics on Europa: Implications for chaos formation. *Journal of Geophysical Research: Planets*, *109*(E3), E03008. https://doi.org/10.1029/2003JE002073

Hansen, U., & Yuen, D. A. (1995). Formation of layered structures in double-diffusive convection as applied to the geosciences. In A. Brandt & H. Fernando (Eds.), *Double-diffusive convection*. American Geophysical Union. Retrieved from http://onlinelibrary.wiley.com/doi/10.1029/GM094p0135/summary

Huppert, H. E., & Moore, D. R. (1976). Nonlinear double-diffusive convection. *Journal of Fluid Mechanics*, *78*(4), 821–854. https://doi.org/10.1017/S0022112076002759

Hussmann, H., Sotin, C., & Lunine, J. (2015). Interiors and evolution of icy satellites. In G. Schubert (Ed.), *Treatise on geophysics* (2nd ed., pp. 605–635). Elsevier. Retrieved from http://www.sciencedirect.com/science/article/pii/B9780444538024001780

Hussmann, H., & Spohn, T. (2004). Thermal-orbital evolution of Io and Europa. *Icarus*, *171*(2), 391–410. https://doi.org/10.1016/j.icarus.2004.05.020

Ingersoll, A. P., & Nakajima, M. (2016). Controlled boiling on Enceladus. 2. Model of the liquid-filled cracks. *Icarus*, *272*, 319–326. https://doi.org/10.1016/j.icarus.2015.12.040

Jia, X., Kivelson, M. G., Khurana, K. K., & Kurth, W. S. (2018). Evidence of a plume on Europa from Galileo magnetic and plasma wave signatures. *Nature Astronomy*, *2*(6), 459–464. https://doi.org/10.1038/s41550-018-0450-z

Journaux, B., Kalousová, K., Sotin, C., Tobie, G., Vance, S., Saur, J., et al. (2020). Large ocean worlds with high-pressure ices. *Space Science Reviews*, *216*(7), 7. https://doi.org/10.1007/s11214-019-0633-7

Kang, W., Mittal, T., Bire, S., Campin, J.-M., & Marshall, J. (2022). How does salinity shape ocean circulation and ice geometry on Enceladus and other icy satellites? *Science Advances*, *8*(29), eabm4665. https://doi.org/10.1126/sciadv.abm4665

Kelley, D. (1987). The influence of planetary rotation on oceanic double-diffusive fluxes. *Journal of Marine Research*, *45*(4), 829–841. https://doi.org/10.1357/002224087788327136

Khurana, K., Kivelson, M. G., Hand, K., & Russell, C. T. (2009). Electromagnetic induction from Europa's ocean and the deep interior. In R. T. Pappalardo, W. B. McKinnon, & K. K. Khurana (Eds.), *Europa*(pp. 381–404). The University of Arizona Press.

King, E. M., Stellmach, S., & Buffett, B. (2013). Scaling behavior in Rayleigh-Bénard convection with and without rotation. *Journal of Fluid Mechanics*, *717*, 449–471. https://doi.org/10.1017/jfm.2012.586

King, E. M., Stellmach, S., Noir, J., Hansen, U., & Aurnou, J. M. (2009). Boundary layer control of rotating convection systems. *Nature*, *457*(7227), 301–304. https://doi.org/10.1038/nature07647

Kivelson, M. G., Khurana, K. K., Russell, C. T., Volwerk, M., Walker, R. J., & Zimmer, C. (2000). Galileo magnetometer measurements: A stronger case for a subsurface ocean at Europa. *Science*, *289*(5483), 1340–1343. https://doi.org/10.1126/science.289.5483.1340

Knobloch, E., Moore, D. R., Toomre, J., & Weiss, N. O. (1986). Transitions to chaos in two-dimensional double-diffusive convection. *Journal of Fluid Mechanics*, *166*(1), 409–448. https://doi.org/10.1017/S0022112086000216

Koh, Z.-W., Nimmo, F., Lunine, J. I., Mazarico, E., & Dombard, A. J. (2022). Assessing the detectability of Europa's seafloor topography from Europa Clipper's gravity data. *The Planetary Science Journal*, *3*(8), 197. https://doi.org/10.3847/psj/ac82aa

Krishnamurti, R. (2009). Heat, salt, and momentum transport in a laboratory thermohaline staircase. *Journal of Fluid Mechanics*, *638*, 491–506. https://doi.org/10.1017/S002211200999098X

Kvorka, J., & Čadek, O. (2022). A numerical model of convective heat transfer in Titan's subsurface ocean. *Icarus*, *376*, 114853. https://doi.org/10.1016/j.icarus.2021.114853

Liang, Y., Carpenter, J. R., & Timmermans, M.-L. (2021). The effect of rotation on double-diffusive convection: Perspectives from linear stability analysis. *Journal of Physical Oceanography*, *51*(11), 3335–3346. https://doi.org/10.1175/jpo-d-21-0060.1

Lowell, R. P., & DuBose, M. (2005). Hydrothermal systems on Europa. *Geophysical Research Letters*, *32*(5), L05202. https://doi.org/10.1029/2005GL022375

Martin, D., Griffiths, R. W., & Campbell, I. H. (1987). Compositional and thermal convection in magma chambers. *Contributions to Mineralogy and Petrology*, *96*(4), 465–475. https://doi.org/10.1007/BF01166691

McCord, T. B., Hansen, G. B., Fanale, F. P., Carlson, R. W., Matson, D. L., Johnson, T. V., et al. (1998). Salts on Europa's surface detected by Galileo's near-infrared mapping spectrometer. *Science*, *280*(5367), 1242–1245. https://doi.org/10.1126/science.280.5367.1242

Melosh, H., Ekholm, A., Showman, A., & Lorenz, R. (2004). The temperature of Europa's subsurface water ocean. *Icarus*, *168*(2), 498–502. https://doi.org/10.1016/j.icarus.2003.11.026

Moll, R., & Garaud, P. (2016). The effect of rotation on oscillatory double-diffusive convection (semiconvection). *The Astrophysical Journal*, *834*(1), 44. https://doi.org/10.3847/1538-4357/834/1/44

Monville, R., Vidal, J., Cébron, D., & Schaeffer, N. (2019). Rotating double-diffusive convection in stably stratified planetary cores. *Geophysical Journal International*, *219*(Supplement 1), S195–S218. https://doi.org/10.1093/gji/ggz347

Newman, F. C. (1976). Temperature steps in Lake Kivu: A bottom heated saline lake. *Journal of Physical Oceanography*, *6*(2), 157–163. https://doi.org/10.1175/1520-0485(1976)006<0157:tsilka>2.0.co;2

Nimmo, F., & Pappalardo, R. T. (2016). Ocean worlds in the outer solar system. *Journal of Geophysical Research: Planets*, *121*(8), 1378–1399. https://doi.org/10.1002/2016JE005081

Patankar, S. V. (1980). *Numerical heat transfer and fluid flow*. CRC Press.

Pearlstein, A. J. (1981). Effect of rotation on the stability of a doubly diffusive fluid layer. *Journal of Fluid Mechanics*, *103*(1), 389–412. https://doi.org/10.1017/S0022112081001390

Postberg, F., Kempf, S., Schmidt, J., Brilliantov, N., Beinsen, A., Abel, B., et al. (2009). Sodium salts in E-ring ice grains from an ocean below the surface of Enceladus. *Nature*, *459*(7250), 1098–1101. https://doi.org/10.1038/nature08046

Radko, T. (2013). *Double-diffusive convection*. Cambridge University Press.

Radko, T., Flanagan, J. D., Stellmach, S., & Timmermans, M.-L. (2014). Double-diffusive recipes. Part II: Layer-merging events. *Journal of Physical Oceanography*, *44*(5), 1285–1305. https://doi.org/10.1175/JPO-D-13-0156.1

Schmalzl, J., Breuer, M., & Hansen, U. (2002). The influence of the Prandtl number on the style of vigoros thermal convection. *Geophysical & Astrophysical Fluid Dynamics*, *96*(5), 381–403. https://doi.org/10.1080/03091920210000499 29

Sharqawy, M. H., V, J. H. L., & Zubair, S. M. (2010). Thermophysical properties of seawater: A review of existing correlations and data. *Desalination and Water Treatment*, *16*(1–3), 354–380. https://doi.org/10.5004/dwt.2010.1079

Shibley, N. C., Timmermans, M.-L., Carpenter, J. R., & Toole, J. M. (2017). Spatial variability of the Arctic Ocean's double-diffusive staircase. *Journal of Geophysical Research: Oceans*, *122*(2), 980–994. https://doi.org/10.1002/2016JC012419

Soderlund, K. (2019). Ocean dynamics of outer solar system satellites. *Geophysical Research Letters*, *46*(15), 8700–8710. https://doi.org/10.1029/2018GL081880

Soderlund, K., Schmidt, B., Wicht, J., & Blankenship, D. D. (2014). Ocean-driven heating of Europa's icy shell at low latitudes. *Nature Geoscience*, *7*(1), 16–19. https://doi.org/10.1038/ngeo2021

Spigel, R. H., & Priscu, J. C. (1998). Physical limnology of the McMurdo Dry Valleys lakes. In *Ecosystem dynamics in a polar desert: The McMurdo Dry Valleys, Antarctica* (pp. 153–187). American Geophysical Union (AGU). https://doi.org/10.1029/AR072p0153

Spigel, R. H., Priscu, J. C., Obryk, M. K., Stone, W., & Doran, P. T. (2018). The physical limnology of a permanently ice-covered and chemically stratified Antarctic lake using high-resolution spatial data from an autonomous underwater vehicle. *Limnology & Oceanography*, *63*(3), 1234–1252. https://doi.org/10.1002/lno.10768

Stellmach, S., Lischper, M., Julien, K., Vasil, G., Cheng, J. S., Ribeiro, A., et al. (2014). Approaching the asymptotic regime of rapidly rotating convection: Boundary layers versus interior dynamics. *Physical Review Letters*, *113*(25), 254501. https://doi.org/10.1103/PhysRevLett.113.254501

Thomson, R. E., & Delaney, J. R. (2001). Evidence for a weakly stratified Europan ocean sustained by seafloor heat flux. *Journal of Geophysical Research: Planets*, *106*(E6), 12355–12365. https://doi.org/10.1029/2000JE001332

Timmermans, M.-L., Marshall, J., Proshutinsky, A., & Scott, J. (2017). Seasonally derived components of the Canada basin halocline. *Geophysical Research Letters*, *44*(10), 5008–5015. https://doi.org/10.1002/2017GL073042

Travis, B., Palguta, J., & Schubert, G. (2012). A whole-moon thermal history model of Europa: Impact of hydrothermal circulation and salt transport. *Icarus*, *218*(2), 1006–1019. https://doi.org/10.1016/j.icarus.2012.02.008

Trumbo, S. K., Brown, M. E., & Hand, K. P. (2019). Sodium chloride on the surface of Europa. *Science Advances*, *5*(6), eaaw7123. https://doi.org/10.1126/sciadv.aaw7123

Turner, J. (1965). The coupled turbulent transports of salt and heat across a sharp density interface. *International Journal of Heat and Mass Transfer*, *8*(5), 759–767. https://doi.org/10.1016/0017-9310(65)90022-0

Turner, J. (1967). Salt fingers across a density interface. *Deep Sea Research and Oceanographic Abstracts*, *14*(5), 599–611. https://doi.org/10.1016/0011-7471(67)90066-6

Vance, S., & Brown, J. (2005). Layering and double-diffusion style convection in Europa's ocean. *Icarus*, *177*(2), 506–514. https://doi.org/10.1016/j.icarus.2005.06.005

Vance, S., & Goodman, J. (2009). Oceanography of an ice-covered moon. In R. T. Pappalardo, W. B. McKinnon, & K. K. Khurana (Eds.), *Europa* (pp. 459–482). The University of Arizona Press.

Vance, S. D., Styczinski, M. J., Bills, B. G., Cochrane, C. J., Soderlund, K. M., Gómez-Pèrez, N., & Paty, C. (2021). Magnetic induction responses of Jupiter's ocean moons including effects from adiabatic convection. *Journal of Geophysical Research: Planets*, *126*(2), e2020JE006418. https://doi.org/10.1029/2020JE006418

Wesseling, P. (1992). *An introduction to multigrid methods*. John Wiley & Sons Inc.

Wong, T., Hansen, U., Wiesehöfer, T., & McKinnon, W. B. M. (2022). Replication Data for: Layering by double-diffusive convection in the subsurface oceans of mid-sized icy satellites. TRR170-DB. https://doi.org/10.35003/OIT7ZO

Yang, Y., Chen, W., Verzicco, R., & Lohse, D. (2020). Multiple states and transport properties of double-diffusive convection turbulence. *Proceedings of the National Academy of Sciences*, *117*(26), 14676–14681. https://doi.org/10.1073/pnas.2005669117

You, Y. (2002). A global ocean climatological atlas of the turner angle: Implications for double-diffusion and water-mass structure. *Deep Sea Research Part I: Oceanographic Research Papers*, *49*(11), 2075–2093. https://doi.org/10.1016/s0967-0637(02)00099-7

Zeng, Y., & Jansen, M. F. (2021). Ocean circulation on Enceladus with a high-versus low-salinity ocean. *The Planetary Science Journal*, *2*(4), 151. https://doi.org/10.3847/psj/ac1114

Zhu, P., Manucharyan, G. E., Thompson, A. F., Goodman, J. C., & Vance, S. D. (2017). The influence of meridional ice transport on Europa's ocean stratification and heat content. *Geophysical Research Letters*, *44*(12), 5969–5977. https://doi.org/10.1002/2017GL072996

Zimmer, C., Khurana, K. K., & Kivelson, M. G. (2000). Subsurface oceans on Europa and Callisto: Constraints from Galileo magnetometer observations. *Icarus*, *147*(2), 329–347. https://doi.org/10.1006/icar.2000.6456

Zolotov, M. Y. (2007). An oceanic composition on early and today's Enceladus. *Geophysical Research Letters*, *34*(23). https://doi.org/10.1029/2007GL031234

Zolotov, M. Y., & Kargel, J. (2009). On the chemical composition of Europa's icy shell, ocean, and underlying rocks. In R. T. Pappalardo, W. B. McKinnon, & K. K. Khurana (Eds.), *Europa* (pp. 431–457). The University of Arizona Press.